Loading Stark-decelerated molecules into electrostatic quadrupole traps

Joop J. Gilijamse, Steven Hoekstra, Nicolas Vanhaecke,* Sebastiaan Y. T. van de Meerakker, and Gerard Meijer†

Fritz-Haber-Institut der Max-Planck-Gesellschaft, Faradayweg 4-6, 14195 Berlin, Germany

(Dated: November 3, 2009)

Beams of neutral polar molecules in a low-field seeking quantum state can be slowed down using a Stark decelerator, and can subsequently be loaded and confined in electrostatic quadrupole traps. The efficiency of the trap loading process is determined by the ability to couple the decelerated packet of molecules into the trap without loss of molecules and without heating. We discuss the inherent difficulties to obtain ideal trap loading, and describe and compare different trap loading strategies. A new "split-endcap" quadrupole trap design is presented that enables improved trap loading efficiencies. This is experimentally verified by comparing the trapping of OH radicals using the conventional and the new quadrupole trap designs.

I. INTRODUCTION

The ability to manipulate and control both the internal (rotation, vibration) and external (velocity, orientation) degrees of freedom of neutral molecules has lead to an increased interest in gas-phase molecular physics. Several books and special issues of journals have recently appeared in which the intense ongoing research efforts in the rapidly emerging field of Cold Molecules are documented [1, 2, 3, 4]. In these references, and in the original literature cited therein, the various experimental routes to produce samples of trapped neutral molecules together with their possible applications and their anticipated or predicted properties are described in detail. One of the experimental approaches is to start with a molecular beam containing internally cold but fast moving neutral molecules, and to then use (a combination of) electric, magnetic or radiative fields to bring these molecules to a standstill and to confine them in a trap [5].

Deceleration of a beam of neutral molecules was first demonstrated on metastable CO molecules using an array of electric fields in a so-called Stark decelerator [6]. The decelerated molecules can subsequently be loaded and confined in a variety of traps. Electric field traps with a quadrupole geometry, originally proposed by Wing for Rydberg atoms [7], offer the steepest and deepest confining potentials, and have resulted, for instance, in the trapping of ND_3 molecules [8] and OH [9] radicals. Traps with other field geometries have been developed and tested as well. A four-electrode trap geometry that combines a dipole, quadrupole and hexapole field has been tested using decelerated ND_3 molecules [10]. Confinement of Stark-decelerated OH radicals in combined magnetic and electric fields [11], as well in a magnetic trap consisting of rare-earth magnets [12], has recently been demonstrated. With the Stark deceleration and trapping technique, samples of cold molecules that are ideally suited for the measurement of the properties of individual molecules, like lifetimes of metastable states, are now routinely produced [13, 14, 15]. At present, the densities in the trap are not high enough to study collective effects, however, as the densities are still too low for collisions to occur between the trapped molecules on the timescale of the trap lifetime. Higher number densities are required if one wants to apply evaporative or sympathetic cooling to increase the phase-space density of the sample of trapped molecules, and optimizing the density of trapped molecules therefore remains an important goal.

To reach the highest possible densities of molecules in the trap, the deceleration and trap-loading process should be performed with the lowest possible losses. During the deceleration process, low losses are assured by the concept of phase stability; the motion of the molecules through the decelerator is as if they were trapped in a travelling potential well [16]. Although coupling of the transverse and the longitudinal motion in the decelerator can lead to loss of molecules [17, 18], these losses can be completely avoided when an improved mode of operation of the decelerator is used [19]. The concept of phase-stability no longer holds when the molecules become too slow, in particular at velocities that are required in the trapping and trap loading region. The coupling of the decelerated packet into the trap is therefore usually accompanied by significant losses; the packet of slow molecules is not kept together sufficiently well in six-dimensional phase-space upon entering the trap. In this paper, the origin of the difficulty to obtain efficient trap loading after Stark deceleration is described in detail. We compare the different strategies that have been implemented in our laboratory in recent years to optimize the loading of Stark decelerated molecules in electrostatic quadrupole traps. We present a new "split-endcap" quadrupole trap design that reduces the losses during trap loading, with-

*Present address: Laboratoire Aimé Cotton, CNRS, Bât 505, Université Paris-Sud, 91405 Orsay, France.

†Author to whom correspondence should be sent. Electronic mail: meijer@fhi-berlin.mpg.de

out affecting the shape and depth of the trapping potential. The improved trap-loading is experimentally demonstrated by comparing the signal of OH radicals in the split-endcap quadrupole trap, with that in a conventional quadrupole trap.

II. LOADING OF ELECTROSTATIC QUADRUPOLE TRAPS

A trap can only confine molecules that have a position and velocity that are within the so-called acceptance of the trap. The position and velocity distribution of the beam that exits the decelerator is called the beam emittance of the decelerator. In the ideal trap design, the (6D) beam emittance of the Stark decelerator is perfectly mapped onto the (6D) acceptance of the trap [20]. In general, the acceptance of the trap can differ in size and shape from the emittance of the decelerator. The shape of the longitudinal acceptance in a quadrupole trap is identical to that of the transverse acceptance, and there is only a geometric factor relating the size of the two. For the packet of slow molecules that exits the decelerator, however, the beam emittance can be rather different in the longitudinal and each of the transverse directions. In principle, a good 6D match can be achieved by installing appropriate focusing elements and free flight sections between the decelerator and the trap that allow for independent control over the longitudinal and transverse motion of the molecules. A pulsed hexapole can be used, for instance, to image the transverse phase-space distribution of the decelerated beam onto the transverse trap acceptance. In the longitudinal direction, this can be achieved when a buncher is used [21]. Although these elements would allow for a good phase-space matching, in practice there are also disadvantages to this approach. Most importantly, these elements significantly increase the distance between the decelerator and trap. In view of the low longitudinal velocity that is required for trap loading (typically 20 m/s or less at the exit of the last deceleration stage, just before the loading), the packet of molecules will spatially expand significantly in the free flight sections between the elements. This will inevitably lead to a large loss of molecules as only a limited part of the beam can be manipulated and loaded into the trap. This was indeed observed in the initial trapping experiments with ND_3 molecules where a short hexapole [8] or a bunching element [20] were installed between the decelerator and trap to allow for some phase-space manipulation of the decelerated packet upon trap loading. In more recent trapping experiments with OH radicals, the more pragmatic approach to install the trap as close as possible to the exit of the decelerator was followed [22]. Although the possibility to influence the phase-space distribution of the packet is compromised, this strategy reduced the losses during the trap loading significantly. The problems inherent to efficient trap loading have already been discussed in the first trapping experiments of

OH radicals [9]. It was observed then that the signal of the trapped OH molecules was optimal when a packet of molecules was loaded into the trap with a velocity that is actually too high. The packet spreads out less upon entering the trap, but only comes to a standstill past the center of the trap. This leads to a donut-shape longitudinal phase-space distribution that basically fills the entire trapping volume. The impossibility to optimize simultaneously the number and temperature of the trapped molecules in this trap design was also discussed in an experiment where the decelerator and trap were optimized using evolutionary strategies [23].

III. MOTION OF MOLECULES DURING TRAP LOADING

To appreciate the problems associated with the efficient loading of Stark-decelerated molecules into an electrostatic trap, a more quantitative discussion of the trap loading procedure is required. In this section, a number of trajectory calculations is presented that illustrate the problems that can occur during the trap loading process. Different trap loading procedures are discussed, with emphasis at first on the evolution of the longitudinal phase-space distribution of the packet of molecules during the trap loading process. Trap loading procedures that can be used with the conventional quadrupole trap are discussed in section III A; the new split-endcap quadrupole trap design is presented in section III B. An experimental comparison of the efficiency of these different trap loading strategies is presented in section III C. In section IV, a discussion of the evolution of the transverse phase-space distribution upon trap loading is given.

A. Conventional quadrupole trap

The geometrical details of the conventional quadrupole trap that has been used so far in our experiments are depicted in figure 1, and have been described in detail elsewhere [22]. The figure shows a cut of the cylindrically symmetric trap, consisting of a ring electrode and two parabolic endcaps. The ring electrode is centered 21 mm downstream from the last electrodes of the decelerator, and has an inner radius R of 10 mm. The two hyperbolic endcaps have a half-spacing of $R/\sqrt{2}$. The 4 and 6 mm diameter openings in the left and right endcap allow for the entrance of the molecules and for the outcoupling of the fluorescence light, respectively. The last three electrode pairs of the Stark decelerator are shown schematically; in reality they are placed alternatingly in orthogonal transverse directions.

A pictorial presentation of the principle of the trap loading process is shown in figure 2. The parameters that are used in this figure apply to a typical OH trapping experiment, and are for a Stark decelerator and trapping machine that is operational in our laboratory [22].
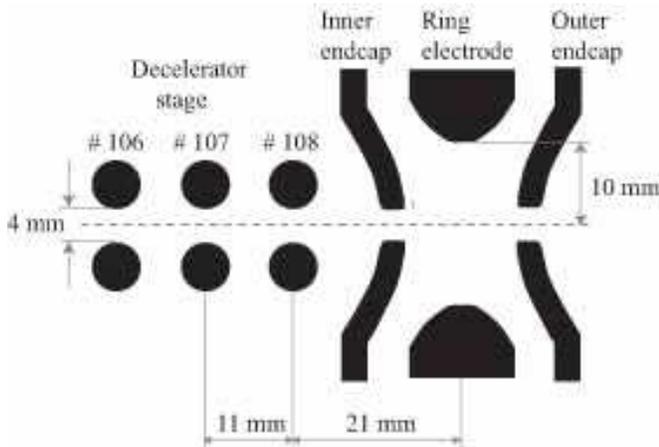
FIG. 1: Schematic representation of the geometry of the last stages of the decelerator and the trap region. The conventional electrostatic quadrupole trap consists of two hyperbolic endcaps and a ring electrode.

FIG. 2: Voltage configurations (top), corresponding potential energy curves for OH molecules along the beam axis (middle), and simulated longitudinal phase-space distributions (bottom) at various stages of the trap loading procedure.

The voltages applied to the individual electrodes in the various stages of the loading sequence are shown in the top of this figure, and the corresponding potential energy curves for an OH molecule that travels along the beam axis are shown directly underneath. The part of the potential that the synchronous molecule [16] experiences during the loading process is indicated by the thick lines. In the loading configuration a voltage of 10 kV, 15 kV and -15 kV is applied to the left endcap, ring electrode and right endcap, respectively. This creates a quadratic loading potential that allows a maximum velocity of 14.9 m/s for the OH radicals at the exit of the decelerator in order to come to a standstill at the trap center. The last stage of the decelerator switches off when the synchronous molecule has reached position A. At this time, the electrodes are switched into the so-called *loading* configuration. Molecules experience the potential corresponding to this configuration while the synchronous molecule moves from position A, via position B, to position C. When the synchronous molecule has finally come to a standstill at position C, the trap center, the voltages on the electrodes are switched to the *trapping* configuration. In the lower panel of figure 2, the evolution of the longitudinal phase-space distribution of the decelerated packet is shown, as it results from numerical simulations of the trap loading process. The distributions are shown at the times at which the synchronous molecule has reached the positions A, B and C. These times are also referred to as times A, B and C. The right-most panel shows the phase-space distribution of the cloud after 20 ms of trapping.

At time A the packet occupies a region in longitudinal phase-space with a velocity spread of 7 m/s (FWHM), centered around a velocity of 15 m/s. After the switching on of the loading potential, this packet first has to overcome a small potential hill in the region in between position A and position B. Since the velocity spread is
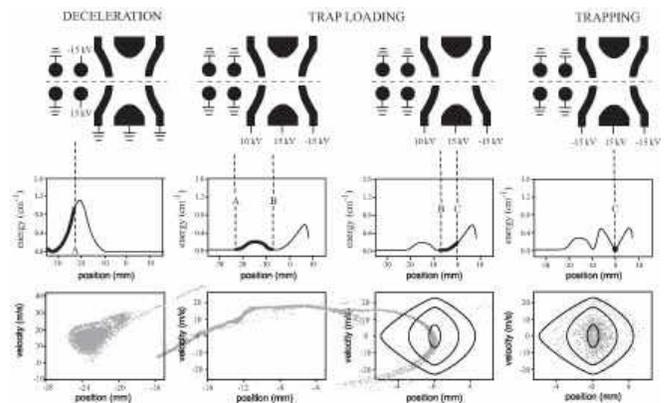
relatively large, a sizeable part of the molecules does not possess enough kinetic energy to overcome this barrier and is reflected, resulting in molecules with negative velocity in the phase-space distribution at time B (second graph from the left in the lowest panel in figure 2). From time B on, molecules are decelerated on the harmonic loading potential and rotate in phase-space around the synchronous molecule. This results in a rather poor overlap of the distribution of molecules with the trap acceptance – that is shown as an overlay – at time C. A large fraction of the molecules is not within the trap acceptance, and will not be confined when the trapping potential is switched on.

In the loading process as sketched above, a substantial fraction of the molecules is reflected by the small "pre-bump" (between A and B) in front of the actual loading potential. In order to reduce the losses associated with this reflection the voltage on the first end-cap electrode in the loading configuration can be lowered. This approach has indeed also been used in the past [9] and has been demonstrated to improve the efficiency of the loading process. A disadvantage of this approach, however, is that the reduced voltage lowers the total height of the potential, and that a slower packet of molecules is required to load the trap. In addition, reduction of the voltage on the left endcap distorts the harmonicity of the loading potential.

An alternative approach to prevent losses due to reflection on the prebump in front of the real loading potential, is to switch the trap into the loading configuration only when the synchronous molecule has reached position B. In this case, there is no prebump, and the molecular packet progresses in free flight to the trap region. This procedure is sketched in figure 3. After the molecules are decelerated to 15 m/s and exit the decelerator at time A, all voltages are switched off, leaving the packet in a field-free region. At time B the mean velocity of the packet is still 15 m/s, but the distribution

is stretched in position. At time B, the loading configuration of the trap is switched on and the molecules are decelerated to a mean velocity of zero at time C, where the molecules are subsequently trapped.
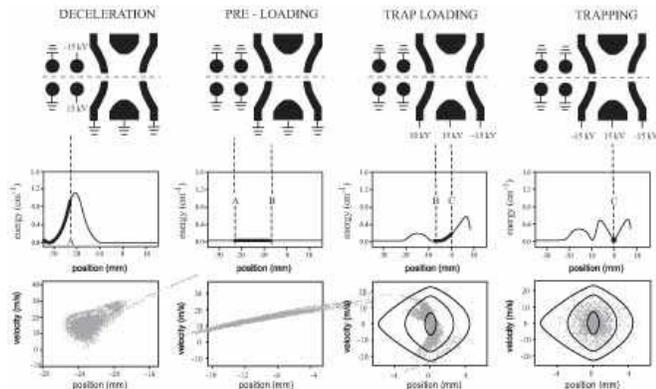
FIG. 3: Voltage configurations as applied in the loading sequence including a free flight section (top). Corresponding potential energy curves for OH molecules along the beam axis (middle). Simulated longitudinal phase-space distributions at various times during trap loading (bottom).

B. Split-endcap quadrupole trap

In the trap loading strategies that are presented above, the trap is positioned as close as possible to the exit of the Stark decelerator. This is probably always preferred over designs that include additional manipulation elements, but nevertheless the trap loading is unsatisfactory. It appears that an improvement can be obtained if the sequence of potentials that keeps the packet together inside the decelerator can be extended into the trap region. Referring back to figures 2 and 3, the breakdown of this sequence is located between the positions A and B. The basic idea of the split-endcap quadrupole trap design presented here is to create a high potential hill in the region AB that can be used as an additional electric field stage of the decelerator, effectively merging the Stark decelerator with the electrostatic trap. It is noted that this idea has also been implemented in trapping experiments using Stark-decelerated ND_3 molecules, where the trap design that was used allowed for a straightforward implementation of an additional electric field stage [24]. For our cylindrically symmetric quadrupole trap, this merging is achieved by breaking the symmetry of the left endcap. In the new trap design this electrode is replaced by two half endcaps with a small vacuum slit between the two halves. The schematic side and front views of the split-endcap electrodes, are shown in figure 4. A small curvature along the vacuum slit between the two halves of the split-endcap is introduced to improve the transverse focusing properties of the trap (see section IV).

Analogous to figure 3, the voltages that are applied to the electrodes, the on-axis potential energy curves
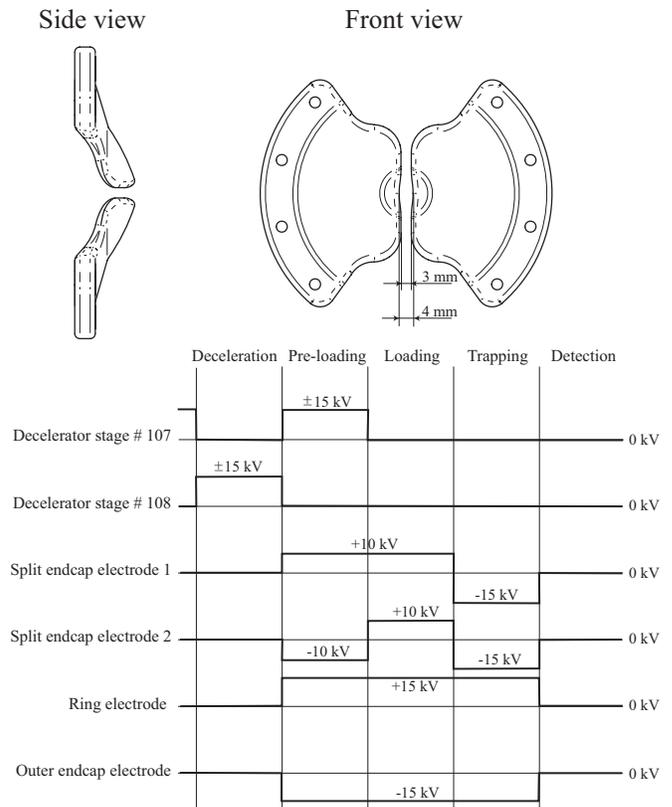
FIG. 4: Side and front views of the split-endcap electrodes. The sequences of high voltage pulses that are applied to all four trap electrodes, as well as to the last two electrode pairs of the decelerator, are graphically shown.

that the synchronous molecule experiences during the trap loading process, and the evolution of the longitudinal phase-space distribution of the packet of molecules, are shown in figure 5. For clarity, the sequence of high voltage pulses that is applied to the last two decelerator stages and to each of the four trap electrodes, are indicated in figure 4. As before, the last pair of electrodes
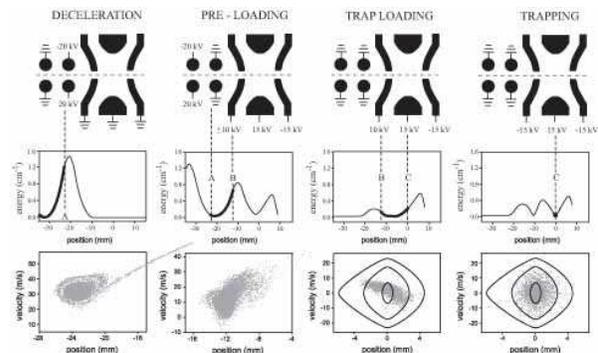
FIG. 5: The Stark decelerator and electrostatic trap are merged in the split-endcap electrode geometry. The potential hill in the region AB is used as an additional deceleration stage.

of the decelerator is switched to ground when the synchronous molecule has reached position A. At this time, both halves of the split-endcap are switched to high voltage (10 kV) of opposite parity, creating a high electric field in between both split-endcap electrodes. Simultaneously, the fore-last set of electrodes of the decelerator are switched to ± 15 kV. In this so-called pre-loading configuration, a potential hill in the region AB is created that is similar in shape to the series of potentials that are present inside the Stark decelerator, and that can be used as an additional deceleration stage. As a result, the forward velocity of the packet of OH radicals at time A can be higher (32 m/s, FWHM 6 m/s) than in the previously discussed trap loading schemes. During this pre-loading configuration, the mean velocity of the packet is reduced to 10 m/s (FWHM 12 m/s). It is evident from the phase-space distribution, that the packet of molecules is kept together much better during this period. When the synchronous molecule has reached position B, the trap loading procedure proceeds in the usual way. The trap can be used in the loading and trapping configuration by switching both halves of the split endcap to the same polarity, first to $+10$ kV and then to -15 kV, respectively. The distance between the two electrodes is small enough that the electric field distribution in the trap is not significantly different from the original situation without a gap, if both halves are switched to the same high voltage. During the loading configuration, the remaining kinetic energy is taken out on the loading slope such that the packet reaches zero velocity in the center of the trap. Then, the trap is switched to the trapping configuration, and the part of the molecular packet that is within the acceptance of the trap stays confined.

It is seen that, compared to the trap loading strategies using the cylindrically symmetric endcap, the longitudinal phase-space distribution is spread out less at the moment the trap is switched on. Even though the phase-space distribution is not perfectly matched to the trap acceptance, almost all molecules are confined within the innermost trap contours.

C. Experiments

The different trap loading strategies presented above are experimentally tested in a Stark deceleration molecular beam machine. A detailed description of this machine, as well as of the production and detection of OH radicals, is given elsewhere [22]. To experimentally study the difference in trap loading efficiency between the conventional and the split-endcap quadrupole trap, a direct comparison between the old and new trap loading approaches is required under otherwise identical conditions, i.e., without removing and re-installing trap electrodes. For this, the original cylindrically symmetric left endcap is replaced by the two split-endcap electrodes. With the split-endcap quadrupole trap in place, trap loading measurements that resemble the old trap loading approach

are still possible when the same high voltage pulses are applied to both halves of the split-endcap. Both split-endcap electrodes, the ring electrode and the outer endcap electrode are individually suspended and connected to an own set of high voltage switches. To enable the switching between voltages of different amplitude and polarity (note that the latter is required for both split-endcap electrodes) a number of high voltage switches are configured in series, i.e., the output of one switch is connected to one of the input ports of the next switch.

For the three trap loading strategies, the loading of the molecules into the trap is experimentally studied by terminating the trap loading sequence at different stages of the trap loading procedure, and by recording the time-of-flight profiles of the slow packet of OH radicals at the center of the trap. In agreement with earlier findings, the first strategy mentioned in section III A was found to be very inefficient and resulted in a poor signal-to-noise ratio in the experiments. These measurements are not shown here. The experimental results that are obtained when the second loading strategy is followed, in which the small potential barrier in the region AB is eliminated by inserting a free-flight section (figure 3), are presented on the left-hand side in figure 6. The Stark decelerator
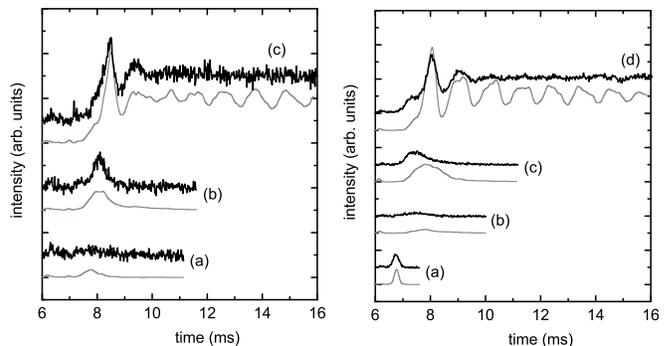
FIG. 6: Time-of-flight profiles of OH radicals at different stages of the trap loading procedure that is depicted in figure 3 (left) and in figure 5 (right). The profiles that are obtained from three-dimensional trajectory simulations of the experiment are shown underneath the experimental profiles. The experimental and simulated profiles are given a vertical offset for clarity.

is programmed to produce a packet of OH radicals with an average forward velocity of 15 m/s. In curve (a) the time-of-flight profile is shown of the packet that exits the decelerator, i.e., the trap loading procedure is stopped after the last stage of the decelerator is switched off. In this curve, the signature of the slow packet of molecules is hardly visible. This is due to the low forward velocity of 15 m/s (FWHM 6 m/s) of the packet, and the spreading out of this packet while flying to the trap center. In curve (b) the time-of-flight profile is shown that is observed when the "loading" part of the trap loading procedure is included. The packet comes to a standstill in the center of the trap, 8.0 ms after production. The higher signal intensity compared to curve (a) is due to the

improved focusing properties when the loading potential is present. Finally, in curve (c), the full trap loading sequence is used. After switching on of the trapping potential, a large increase of signal followed by a damped oscillation is observed. The time-of-flight profiles that result from three dimensional trajectory simulations are shown underneath the experimental profiles. Satisfactory agreement is obtained for all curves, and the relative signal intensities of the different profiles are reproduced rather well. The difference between the simulated and measured curves regarding the damping of the oscillation is discussed later in section IV.

On the right-hand side of figure 6 the measured time-of-flight profiles are shown that correspond to the loading strategy when the split-endcap electrodes are used as an additional deceleration stage. The "deceleration", "loading", and "trapping" profiles are shown in curves (a), (c), and (d), respectively. The additional profile that corresponds to the "pre-loading" configuration, is shown in curve (b). The packet of molecules that exits the decelerator has a forward velocity of 32 m/s with a velocity spread of 7 m/s, and arrives at the trap center 6.8 ms after its production. Due to the higher forward velocity, the packet spreads out less, and the signature of the slow packet is clearly visible in the time-of-flight profile. When the pre-loading configuration is added to the trap loading sequence, curve (b) is obtained. The packet arrives later at the trap center, and the arrival time distribution is broader. This reflects the lower forward velocity of 10 m/s. This very low forward velocity also explains the reduced signal intensity; the packet of molecules expands significantly when the voltages on the trap electrodes are switched off in this time-of-flight measurement. The packet is brought to a standstill at the center of the trap when the loading part is added (curve (c)). The loading potential prevents the packet from spreading out, and the signal intensity of the stopped molecules is higher again. Curve (d) corresponds to the full trap loading sequence. Again, a large increase of signal followed by a damped oscillation is observed when the trap is switched on. The time-of-flight profiles that result from three dimensional trajectory simulations are shown underneath the experimental profiles. Again, satisfactory agreement is obtained for all curves, although the slow packet in curves (b) and (c) arrives earlier in the experiment than in the simulation. This is indicative of an over-estimate of the pre-loading potential in the simulations. Deviations originate from misalignments of the trap electrodes in the experiment, and from slight differences between the actual and simulated shapes of the electrodes.

D. Discussion

The intensity of the fluorescence signal from the trapped sample of molecules that is obtained when the three different trap loading strategies are used can be directly compared. The experimental results are summarized in Table I. In this Table, the three loading strategies are referred to as "conventional loading", "free flight loading", and "split-endcap loading", and the figures in which these loading strategies are explained are given. The fluorescence intensities are normalized to the fluorescence intensity that is obtained using the conventional trap loading strategy.

TABLE I: Comparison of experiments and simulations using different trap loading strategies.

Trap loading strategy	Described in Figure	Signal int. (Exp.)	Efficiency (Sim.)	N (Sim.)	T (Sim.)
Conventional	2	1.0	15 %	1.0	59 mK
Free flight	3	4.0	27 %	1.8	51 mK
Split-endcap	5	8.9	27 %	1.9	48 mK

It is seen that with the conventional quadrupole trap, the efficiency of trap loading is increased by a factor 4 if a free flight section is included in the loading sequence. Another factor of 2.2 is gained if the left end-cap electrode is replaced by split-endcap electrodes. It is noted that this value represents a lower limit of the gain, as the present experiments are all performed with the split-endcap electrodes in place. Compared to the spherically symmetric endcap, that has a mere 4 mm diameter opening, the slit offers a higher probability for the molecules to enter the trap.

It is interesting to compare these experimental findings with trap loading efficiencies that result from three dimensional trajectory simulations. In general, it is difficult to obtain a quantitative agreement between three dimensional trajectory simulations and experimental results for trapping experiments. This is in part due to the low velocity of the molecules during the trap loading process, and hence their sensitivity to the exact details of the potentials involved, and in part due to the complex shapes of the trap electrodes. Nevertheless, these simulations are helpful to yield a qualitative understanding of the trap loading process.

Three dimensional trajectory simulations have been performed for all trap loading strategies. The calculated trap loading efficiencies, defined as the fraction of the molecules that exit the decelerator and that are still confined in the trap 20 ms after the trap has been switched on, are presented in the fourth column of Table I. For a direct comparison with the experimental findings, however, the ratio between the absolute number of molecules that are confined in the trap is of relevance. This ratio can differ from the ratio of the efficiencies, as the molecular packet has a different velocity in the last stage of the decelerator for the different loading strategies. The resulting number of molecules, normalized to the number that is obtained using the "conventional" loading strategy, is given in the fifth column of Table I. Finally, the temperature T of the trapped sample of molecules that follows from these simulations is given in the last column of Table I. This temperature is defined using the average kinetic energy of the molecules $E_{kin} = 3/2 k_B T$, where

k_B is the Boltzmann constant.

It is seen that in the simulations, the performance of the "conventional" trap loading strategy is worse than the "free flight" or "split-endcap" loading strategy, in qualitative agreement with the experimental findings. In contrast, the simulations do not predict the improved loading efficiency for the "split-endcap" compared to the "free flight" strategy that was found experimentally (see table I), and that was expected from the one dimensional simulations presented in figures 3 and 5. This somewhat surprising result indicates that the transverse focusing properties of the split-endcap electrodes can diminish the gain that is obtained in the longitudinal direction, as will be discussed in detail below.

IV. TRANSVERSE MOTION DURING TRAP LOADING

Analogous to the evolution of the longitudinal phase-space distribution during the trap loading process, the phase-space distribution in both transverse directions can be derived from the three dimensional trajectory simulations. These are shown for the split-endcap loading strategy in figure 7. The transverse coordinate y (top
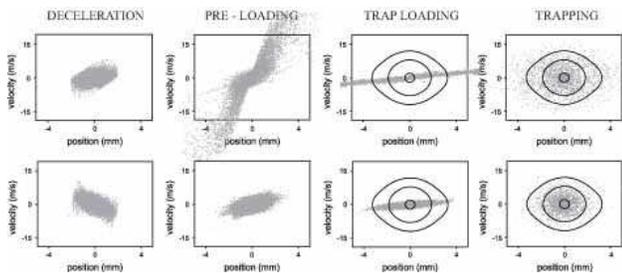
FIG. 7: Transverse (y (top) and z (bottom)) phase-space distributions at various stages of the experiment. These transverse phase-space snapshots belong to the longitudinal distributions presented in figure 5.

panels) is defined along the long axis of the last electrode pair. The transverse coordinate z (lower panels) is defined perpendicular to that axis. As can be seen on the left side of figure 7, the molecular packet has transverse dimensions of 4x4 mm^2 at the exit of the decelerator, given by the distance between the electrodes in each electrode pair. The split-endcap electrodes face each other in the y direction and create a pre-loading field that is perpendicular to the field of the last deceleration stage. Therefore, as the packet travels in the pre-loading field it is not only decelerated in the longitudinal (x) direction, but also gets strongly focused in the y direction. The exact strength of this focusing force depends on the longitudinal position of the molecules, resulting in a non-uniform rotation of the phase-space distribution. During the "pre-loading" configuration, the molecules hardly experience focusing forces in the z direction (the direction along the slit of the split-endcap electrodes), and in this

direction the phase-space distribution evolves more-or-less like in free flight. When the packet progresses on the subsequent (cylindrically symmetric) loading potential, the molecules get focused in the y and z direction equally strong. These focusing forces, however, are limited, and in addition to a rotation in phase-space, the packet also elongates spatially. The resulting phase-space distributions at the moment the trap is switched into the "trapping" configuration are shown in the third panel of figure 7.

It is clear from these distributions that, in contrast to the longitudinal phase-space overlap, the phase-space overlap with the transverse trap acceptance is rather poor. In the y-direction, the focusing force during the "pre-loading" configuration has been too strong. A significant part of the molecules pass through a focus, resulting in a large velocity spread when the packet enters the "loading" potential. This large velocity spread is transferred into a large position spread during the "loading" part of the sequence. In the z-direction, however, the focusing forces are too weak. The packet spreads out significantly, also resulting in a large position spread at the time the trap is switched on.

The (transverse) mismatch between the phase-space distribution of the molecular packet and the trap acceptance at the moment the trapped is switched on can also be inferred from the time-of-flight profile in figure 6(d), that is shown again in the upper curve of figure 8. Pronounced oscillations in the signal intensity of the trapped molecules are observed in the first milliseconds after the trap has been switched on. These oscillations result from fluctuations in the density of molecules within the detection volume, that can be observed if the detection volume is considerably smaller than the total volume of the trap. The detection volume is given by the 4 mm diameter of the detection laser, that crosses both transverse coordinates y and z under an angle of 45°, and the opening angle of the detection zone, given by the 6 mm diameter opening in the right endcap. In figure 8 it is shown that the fluctuations in density are mainly caused by the rotation of the phase-space distribution of the packet in the transverse directions. At time I, the time that the molecular packet arrives in the trap center and the trap is switched on, the packet is longitudinally and transversely (almost) velocity-focused; the packet is spatially large (3x10x4 mm^3) and has a relative small velocity spread (FWHM) of about 7, 5, and 2 m/s in the x, y, and z direction, respectively. As can be seen from the top of the figure this situation corresponds to a relative low LIF signal in the time-of-flight profile, since a large fraction of the molecules is located in the region of the trap that is not overlapped with the detection laser. At time II, the situation is exactly opposite. The phase-space distributions have rotated and most molecules are located in the center of the trap. The packet has a size of 1x2x2 mm^3 and a relatively high velocity spread of 21, 18, and 8 m/s in the x, y, and z direction, respectively. This situation corresponds with an intense LIF signal. The phase-space
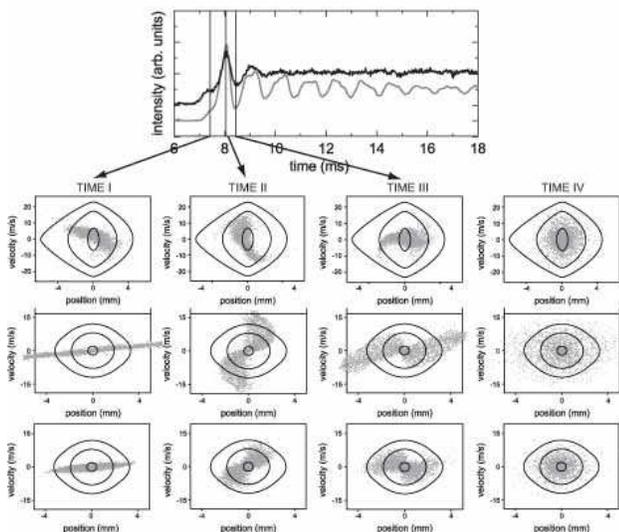
FIG. 8: Phase-space distributions in the longitudinal (x, top panel) and in both transversal (y, middle panel; z, lower panel) directions at different points in time, indicated with vertical lines in the time-of-flight profile shown on the top. Time I is the time of switching from the loading to the trapping potential. Time II and III correspond to the first maximum and minimum of the oscillations as observed in the time-of-flight profile of the trapping experiment, respectively. Time IV is 20 ms after the trap has been switched on.

distributions after 20 ms of trapping, shown in figure 8 (time IV), show that the packet no longer has a clear structure in phase-space and the trap acceptance is homogeneously filled. The size of the molecular packet and the ratio between the velocity distributions in the three directions are now given by the shape of the phase-space acceptance of the trap. The spatial distribution at this moment is $2x2x2$ mm^3, the velocity distribution 10, 8, and 7 m/s in the x, y, and z direction, respectively. This "steady-state" situation is reached as a result of the coupling of the motion in all coordinates. The number of oscillations that is actually seen in the simulated time-of-flight profile critically depends on the details of the implementation of the detection zone and the LIF collection optics in the simulation, and differs from the number of oscillations that is seen in the experiment.

V. CONCLUSIONS

In this paper, the efficiency of the loading of Stark-decelerated molecular beams into electrostatic quadrupole traps has been studied. These studies have been triggered by high losses that have been observed during the trap loading process in previous Stark deceleration and trapping experiments. These losses occur because it is difficult to keep the molecular packet together in the region between the end of the Stark decelerator and the first electrode of the quadrupole trap. A new split-endcap quadrupole trap, in which the cylindical symmetry of a quadrupole trap is broken, is presented. This trap design allows for a continuation of the sequence of potentials that are present inside the Stark decelerator into the trap region, and effectively merges the exit of the Stark decelerator with the electrostatic quadrupole trap. The improved performance of this split-endcap quadrupole trap has been experimentally verified by comparing the electrostatic trapping of OH radicals using the new and conventional quadrupole traps. Compared to the most successful loading strategy that has been obtained in a quadrupole trap with the conventional electrode design, an improvement in loading efficiency of a factor 2.2 has experimentally been observed.

Three dimensional trajectory simulations of the trap loading process reveal that in its current implementation, however, the advantages of the split-endcap design are not yet fully exploited. In the region between the Stark decelerator and the entrance of the trap, the focusing of the molecular packet in one of the two transverse directions is larger than desired, diminishing the gain that is achieved in the longitudinal direction. The main lesson learnt from these simulations is that the exact shape of the split-endcap electrodes in the region of the slit is very critical to the success of the split-endcap quadrupole trap. The slit should be designed such that, prior to passing the slit, the molecules experience a strong deceleration force but only modest transverse focussing forces. This can, for instance, be accomplished with split-endcap electrodes that are designed to form an entrance opening slit with a more conical shape. For future implementations of quadrupole traps that are based on the split-endcap loading strategy, the critical interplay between longitudinal and transverse forces during trap loading needs to be thoroughly investigated using three dimensional trajectory simulations.

[1] I. Smith, ed., *Low Temperatures and Cold Molecules* (Imperial College Press, 2008).

[2] R. Krems, W. Stwalley, and B. Friedrich, eds., *Cold Molecules: Theory, Experiment, Applications* (Taylor and Francis, 2009).

[3] L. Carr and J. Ye, eds., *Focus on Cold and Ultracold Molecules* (special issue in New Journal of Physics, 2009).

[4] *Faraday Discussion 142: Cold and Ultracold Molecules*

(2009).

[5] S. Y. T. van de Meerakker, H. L. Bethlem, and G. Meijer, Nature Physics **4**, 595 (2008).

[6] H. L. Bethlem, G. Berden, and G. Meijer, Phys. Rev. Lett. **83**, 1558 (1999).

[7] W. H. Wing, Phys. Rev. Lett. **45**, 631 (1980).

[8] H. L. Bethlem, G. Berden, F. M. H. Crompvoets, R. T. Jongma, A. J. A. van Roij, and G. Meijer, Nature **406**, 491 (2000).

[9] S. Y. T. van de Meerakker, P. H. M. Smeets, N. Vanhaecke, R. T. Jongma, and G. Meijer, Phys. Rev. Lett. **94**, 023004 (2005).

[10] J. van Veldhoven, H. L. Bethlem, M. Schnell, and G. Meijer, Phys. Rev. A **73**, 063408 (2006).

[11] B. C. Sawyer, B. L. Lev, E. R. Hudson, B. K. Stuhl, M. Lara, J. L. Bohn, and J. Ye, Phys. Rev. Lett. **98**, 253002 (2007).

[12] B. C. Sawyer, B. K. Stuhl, D. Wang, M. Yeo, and J. Ye, Phys. Rev. Lett. **101**, 203203 (2008).

[13] S. Y. T. van de Meerakker, N. Vanhaecke, M. P. J. van der Loo, G. C. Groenenboom, and G. Meijer, Phys. Rev. Lett. **95**(1), 013003 (2005).

[14] J. J. Gilijamse, S. Hoekstra, S. A. Meek, M. Metsälä, S. Y. T. van de Meerakker, G. Meijer, and G. C. Groenenboom, J. Chem. Phys. **127**, 221102 (2007).

[15] S. Hoekstra, J. J. Gilijamse, B. Sartakov, N. Vanhaecke, L. Scharfenberg, S. Y. T. van de Meerakker, and G. Meijer, Phys. Rev. Lett. **98**(13), 133001 (2007).

[16] H. L. Bethlem, G. Berden, A. J. A. van Roij, F. M. H. Crompvoets, and G. Meijer, Phys. Rev. Lett. **84**, 5744 (2000).

[17] S. Y. T. van de Meerakker, N. Vanhaecke, H. L. Bethlem, and G. Meijer, Phys. Rev. A **73**(2), 023401 (2006).

[18] B. C. Sawyer, B. K. Stuhl, B. L. Lev, J. Ye, and E. R. Hudson, Eur. Phys. J. D **48**, 197 (2008).

[19] L. Scharfenberg, H. Haak, G. Meijer, and S. Y. T. van de Meerakker, Phys. Rev. A **79**, 023410 (2009).

[20] H. L. Bethlem, F. M. H. Crompvoets, R. T. Jongma, S. Y. T. van de Meerakker, and G. Meijer, Phys. Rev. A **65**(5), 053416 (2002).

[21] F. M. H. Crompvoets, R. T. Jongma, H. L. Bethlem, A. J. A. van Roij, and G. Meijer, Phys. Rev. Lett. **89**(9), 093004 (2002).

[22] S. Y. T. van de Meerakker, N. Vanhaecke, and G. Meijer, Ann. Rev. Phys. Chem. **57**, 159 (2006).

[23] J. J. Gilijamse, J. Küpper, S. Hoekstra, N. Vanhaecke, S. Y. T. van de Meerakker, and G. Meijer, Phys. Rev. A **73**(6), 063410 (2006).

[24] M. Schnell, P. Lützow, J. van Veldhoven, H. Bethlem, J. Küpper, B. Friedrich, M. Schleier-Smith, H. Haak, and G. Meijer, J. Phys. Chem. A **111**, 7411 (2007).